Pis'ma v ZhETF, vol. 96, iss. 2, pp. 123 – 127

Spectral properties of LiFeAs: an LDA+DMFT study

S. L. Skornyakov[+], D. Y. Novoselov[+], T. Gürel[×], V. I. Anisimov[+*]*

[+] *Institute of Metal Physics UD of the RAS, 620990 Yekaterinburg, Russia*

[*] *Ural Federal University, 620002 Yekaterinburg, Russia*

[×] *Department of Physics, Namik Kemal University, 59030 Tekirdağ, Turkey*

Submitted 17 May 2012
Resubmitted 20 June 2012

Spectral properties of LiFeAs superconductor are investigated within the LDA+DMFT method. Calculated distribution of the spectral weight in the $\mathbf{k}$-space is in good agreement with angle-resolved photoemission (ARPES) spectra. Calculated effective electron mass enhancement factor $m^*/m \approx 3$ is close to the one estimated from comparison of density-functional theory results with ARPES spectra. Our results demonstrate that inclusion into consideration of dynamical Coulomb correlations between the electrons plays a key role in understanding of the spectral properties of LiFeAs.

Discovery of high-temperature superconductivity in layered iron pnictides [1] has initiated an increasing interest to this class of compounds [2–12]. The pnictides represent a completely new class of superconductors with critical temperatures higher than for the conventional BCS superconductors but lower than for the high-T_c cuprates. Since the mechanism of superconductivity in pnictides is still not clear, researchers interpret their results trying to find parallels in behaviour of physical properties of the pnictides with other classes of superconducting compounds, especially with the cuprates.

The pnictides and the cuprates crystallize into a layered crystal structures and share a common phase diagram with antiferromagnetic spin-density wave (SDW) appearing below the Neèl temperature. As in the case of cuprates, almost in all pnictide families parent compounds are not superconducting. Superconductivity is associated with suppression of the SDW ordering under pressure or adding electrons via doping with simultaneous transition of the system into a superconducting state. But in the case of cuprates parent compounds are Mott insulators and in the case of pnictides parent systems are metals. Since it is generally accepted that strong Coulomb correlations between Cu electrons are responsible for formation of anomalous properties of the cuprates, investigation of the role of electron-electron interactions is an important issue for understanding of superconducting transition mechanism in the pnictides.

Coulomb correlations in pnictide compounds are intensively studied during last four years. Initially pnictides were considered as strongly correlated systems on the verge of metal-to-insulator transition [3]. Later studies shown that the correlation strength should be classified as moderate [4–6] (i.e. sufficient to cause changes of the excitation spectrum at the Fermi level but still weak to form the Hubbard bands).

Lithium ferroarsenide shows unique spectral and magnetic properties in comparison with the other iron pnictides. First, the stoichiometric compound becomes superconducting under cooling ($T_c = 18$ K [10]) without a need of applying pressure or adding of extra-carriers by means of doping. Second, according to angle-resolved photoemission spectra, unlike other pnictides there is only a poor nesting [11] of the electronic and hole pockets of the Fermi surface (FS) in LiFeAs. As a consequence, spin fluctuations are not as strong as in other pnictide superconductors which, in turn, results in lowering [13, 14] of the critical temperature in LiFeAs.

In this work we investigate the role of Coulomb electronic correlations in formation of the spectral properties of LiFeAs compound within first-principle LDA+DMFT method [15] which combines the local density approximation (LDA) with the dynamical mean-field theory [16] (DMFT). We have calculated the spectral functions $A(\mathbf{k},\omega)$ and the effective electron mass enhancement factor m^*/m, and compare our results with the available ARPES spectra for LiFeAs [11] finding good agreement between the calculated and experimental data.

The realization of LDA+DMFT scheme employed in the present work proceeds in three stages. First, an effective Hamiltonian $\tilde{h}_{\mathbf{k}}$ is constructed in the basis of Wannier functions using converged LDA result. Second, the many-body Hamiltonian $H(\mathbf{k})$ is set up. And the third step includes iterative solution of the corresponding self-consistent DMFT equations.

The effective 16-band Hamiltonian $\tilde{h}_{\mathbf{k}}$ incorporates five Fe $3d$-orbitals and three As $4p$-orbitals for each of the two Fe and As ions per unit cell. The Wannier functions were generated within projection procedure [17] for an energy window including both p- and d-bands. Hence, by construction eigenvalues of the effective Hamiltonian $\tilde{h}_{\mathbf{k}}$ exactly correspond to 16 bands of Fe and As obtained in the full-orbital LDA calculation and hybridization effects between As $4p$- and Fe $3d$-electrons are explicitly taken into account. The LDA calculations were performed with the experimentally determined crystal structure [10] using the Elk full-potential linearized augmented plane-wave (FP-LAPW) code [18]. Parameters controlling the LAPW basis were kept to their default values. To account for the Coulomb interaction energy between d-electrons already present in LDA the dd diagonal elements of the effective Hamiltonian $\tilde{h}_{\mathbf{k}}$ are renormalized by a double counting correction [17] $E_{\mathrm{DC}} = \bar{U}(n_{\mathrm{DMFT}} - 1/2)$,

$$h^{dd}_{\mathbf{k},\alpha\beta} = \tilde{h}^{dd}_{\mathbf{k},\alpha\beta} - E_{\mathrm{DC}}\delta_{\alpha\beta}. \tag{1}$$

Here, n_{DMFT} denotes the total self-consistently calculated number of d-electrons per Fe site obtained within DMFT, and $\bar{U}$ is the average Coulomb parameter for the d shell which includes the effects of inter- and intra-orbital interactions. This form of E_{DC} yields reliable results for transition metal compounds including the pnictide superconductors LaFeAsO, LaFePO, and $BaFe_2As_2$ [5–7]. The pd Hamiltonian to be solved by DMFT then has the form

$$\begin{aligned} H(\mathbf{k}) = \sum_{k,\sigma}(h^{dd}_{\mathbf{k},\alpha\beta} d^{\dagger}_{\mathbf{k}\alpha\sigma} d_{\mathbf{k}\beta\sigma} + h^{pp}_{\mathbf{k},\gamma\sigma} p^{\dagger}_{\mathbf{k}\gamma\sigma} p_{\mathbf{k}\delta\sigma} + \\ + h^{dp}_{\mathbf{k},\alpha\gamma} d^{\dagger}_{\mathbf{k}\alpha\sigma} p_{\mathbf{k}\gamma\sigma} + h^{pd}_{\mathbf{k},\gamma\alpha} p^{\dagger}_{\mathbf{k}\gamma\sigma} d_{\mathbf{k}\alpha\sigma}) + \\ + \sum_{i,\sigma,\sigma'} U^{\sigma\sigma'}_{\alpha\beta} n^{d}_{i\alpha\sigma} n^{d}_{i\beta\sigma'}. \end{aligned} \tag{2}$$

In Eq. (2), the operators $d_{\mathbf{k}\alpha\sigma}$ and $p_{\mathbf{k}\gamma\sigma}$ are Fourier transforms of $d_{i\alpha\sigma}$ and $p_{i\gamma\sigma}$, which annihilate the d- or p-electron with orbital and spin indices $\alpha\sigma$ or $\gamma\sigma$ in the ith unit cell, and $n^{d}_{i\alpha\sigma}$ is the corresponding occupation number operator. The DMFT self-consistent equations were solved iteratively on the Matsubara contour. The DMFT auxiliary impurity problem was solved by the Continuous- time quantum Monte Carlo (QMC) method [19]. The elements of the interaction matrix $U^{\sigma\sigma'}_{\alpha\beta}$ are parametrized by the on-site Coulomb potential U and intraatomic exchange parameter J according to procedure described in [20]. In the present work the interaction parameters $U = 3.5\,\mathrm{eV}$ and $J = 0.85\,\mathrm{eV}$ were calculated according to the constrained DFT method [21]. The DMFT calculations were performed for the paramagnetic phase of LiFeAs at the inverse temperature $\beta = 1/T = 40\ \mathrm{eV}^{-1}$. The local self-energy $\Sigma(\omega)$, which is formally an 16×16 matrix with the only nonzero elements on the diagonal of the dd block, was obtained by means of analytic continuation from imaginary Matsubara frequencies to the real energy axis with the use of Padé approximants [22].

For the multi-orbital problem hybridization effects play a crucial role and the band structure cannot be represented as a superposition of independent bands with given symmetry. In this case the Green's function $G(\mathbf{k},\omega)$ is a matrix in orbital indices defined in each point of the reciprocal space,

$$G(\mathbf{k},\omega) = [\omega + \mu - H(\mathbf{k}) - \Sigma(\omega)]^{-1}, \tag{3}$$

where μ is the self-consistent DMFT chemical potential. The momentum- and orbitally-resolved spectral function $A_i(\mathbf{k},\omega)$ by analogy with the single-orbital case corresponds to diagonal (with respect to the orbitals) elements of the Green's function, $A_i(\mathbf{k},\omega) = -\frac{1}{\pi}G_{ii}(\mathbf{k},\omega)$. The orbitally resolved local spectral function $A_i(\omega)$ is obtained by summation over all contributions within the first Brillouin zone, $A_i(\omega) = \sum_{\mathbf{k}} A_i(\mathbf{k},\omega)$.

Comparison of the orbitally-resolved Fe $3d$ and As $4p$ spectral functions computed within LDA and LDA+DMFT is shown in Fig. 1. Within the LDA all five Fe $3d$-orbitals form a common band in the energy range $(-2.5, +2)\,\mathrm{eV}$ relative to the Fermi level (band width $W \approx 4.5\,\mathrm{eV}$). There is a significant hybridization of the Fe $3d$-orbitals with the As $4p$-orbitals leading to appearance of the Fe $3d$ spectral weight in the energy interval $(-5, -2.5)\,\mathrm{eV}$ where the As $4p$-band is located. Nevertheless, this is not a correlation effect because there are no additional poles emerging due to the self-energy in the Green's function in that energy range, i.e. the corresponding features cannot be interpreted as the Hubbard bands. The overall shape of the LDA spectral functions (including the peaks below and above the Fermi level located in the interval $E_{\mathrm{F}} \pm 2\,\mathrm{eV}$) remains almost unchanged in the presence of the correlations. The only effect of correlations on the spectral properties is substantial renormalization of the spectrum in the vicinity of the Fermi energy so that separation between the peaks in LDA+DMFT becomes approximately three times smaller in comparison with the LDA.

A quantitative measure of electronic correlation strength is provided by enhancement of the effective mass. The mass enhancement coefficient m^*/m is connected with quasiparticle renormalization factor $Z^{-1} = m^*/m$. Here m (m^*) corresponds to the effective band mass in LDA (DMFT) and is related to the dispersion law $\epsilon_{\mathrm{LDA(DMFT)}}(\mathbf{k})$ as $m^{(*)} = \hbar^2 \int d\mathbf{k}[1/\nabla^2_{\mathbf{k}}\epsilon_{\mathrm{LDA(DMFT)}}(\mathbf{k})]$, and $Z = (1 - \frac{\partial\Sigma}{\partial\omega}|_{\omega=0})^{-1}$. In the multiorbital case the

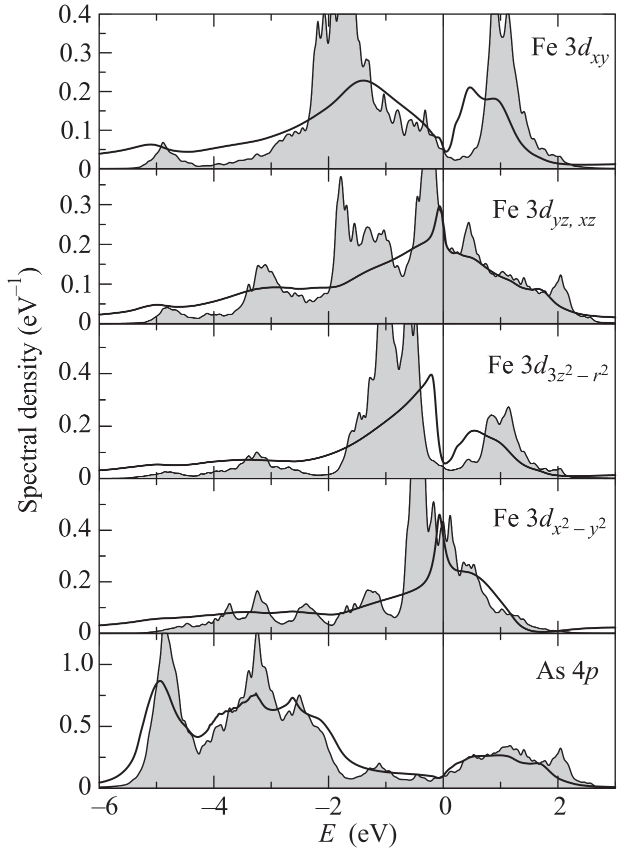

Fig. 1. Orbitally resolved Fe $3d$ and total As $4p$ spectral functions of LiFeAs obtained within LDA+DMFT (straight lines) in comparison with LDA results (shaded areas)

self-energy is a matrix which leads to different m^*/m for different orbitals. Within DMFT approximation the self-energy is momentum-independent and m^*/m describes average renormalization of the bands with given symmetry in the vicinity of the Fermi energy. The calculated effective mass enhancement for each Fe $3d$-orbital are presented in Table. The $d_{x^2-y^2}$ orbital has the largest value of effective mass renormalization ($m^*/m = 4.09$). The smallest value 2.01 corresponds to the d_{xy} orbital. The averaged mass enhancement of 3.03 agrees well with the renomalization factor of 3.01 reported by Borisenko et al. [11] based on comparison of the LDA results and ARPES data. In spite of large m^*/m the compound under investigation should not be treated as a strongly correlated system. According to the scheme introduced in [5], LiFeAs as all other representatives of the pnictide class is a moderately correlated system.

More detailed information on the spectral properties can be extracted from the band structure. The correlated band structure $\epsilon_{\mathrm{DMFT}}(\mathbf{k})$ was computed as poles of

Effective electron mass enhancement m^*/m for different orbitals of the Fe $3d$ shell of LiFeAs

	d_{xy}	$d_{yz,xz}$	$d_{3z^2-r^2}$	$d_{x^2-y^2}$
m^*/m	2.01	3.32	2.41	4.09

the interacting DMFT Green's function [3]. The dispersion curves obtained within DMFT for the large energy interval are shown in Fig. 2 in comparison with the LDA

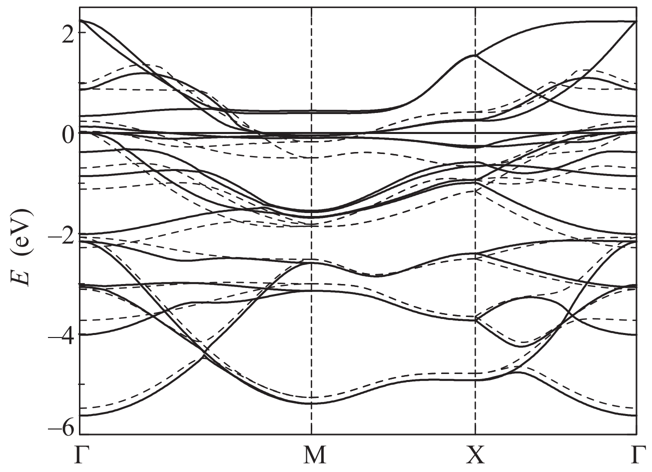

Fig. 2. Energy bands of LiFeAs computed within LDA+DMFT (straight lines) in comparison with the LDA result (dashed lines)

result. As in the analysis of the orbitally resolved densities of states we note that dynamical correlation effects lead to significant narrowing of the band structure in the vicinity of the Fermi energy and the total width of the *pd* complex of bands remains almost unchanged. In Fig. 3 $\epsilon_{\mathrm{DMFT}}(\mathbf{k})$ calculated along ΓXΓ, ΓMΓ, and MXM directions in the Brilloiun zone is shown in comparison with ARPES data of Borisenko et al. [11]. The calculated correlated band structure is in good agreement with experimental intensity map. More specifically, the results of LDA+DMFT calculation reproduce the character of the Fermi surface (position and size of the electronic and hole pockets) and the number of bands crossing the Fermi level. It is also possible to conclude that significant contribution to the spectral weight of the peaks below the Fermi energy is provided by the flat band regions located at -0.1 eV on the Γ-M direction. We also note that near the Fermi energy, i.e., in the energy range from -0.25 to 0 eV where quasiparticles are well defined (real part of the self-energy is a linear function of frequency and imaginary part behaves as $-\omega^2$) this dispersion is very well represented by the scaling relation $\epsilon_{\mathrm{DMFT}}(\mathbf{k}) = \epsilon_{\mathrm{LDA}}(\mathbf{k})/(m^*/m)$, with m^*/m taken as the computed average mass enhancement.

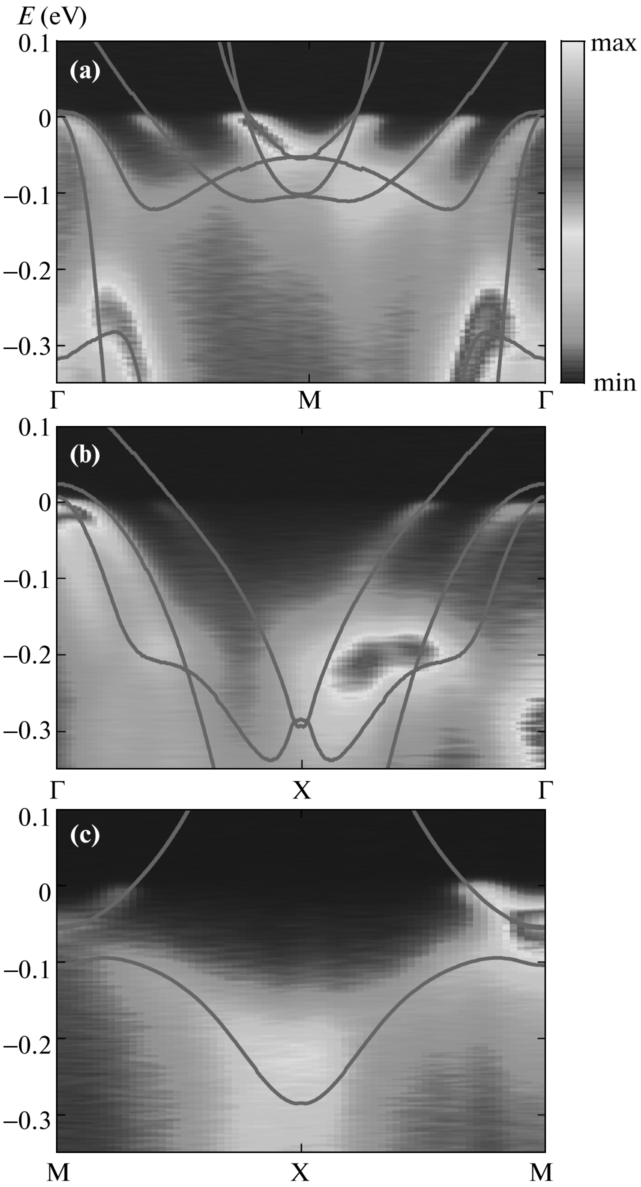

Fig. 3. The band structure of LiFeAs along ΓMG, MXM and ΓXΓ lines of the Brillouin zone (lines) in comparison with ARPES data [11] (contours)

In Fig. 4 the Fermi surface region (that is $A(\mathbf{k},\omega = 0)$) is shown as a contour plot. The **k**-vectors were chosen belonging to the plane defined by Γ, X, and M points of the reciprocal space. The computed FS has several pronounced features wich form and position is very close to the ones observed in experimental spectrum of Borisenko et al. [11]. There is a barrel-like FS centered at the Γ point with high-intensity region inside. The M point is surrounded by a square cylinder with rounded edges. The shape of this FS is very different from that surrounding the Γ point. Thus these two

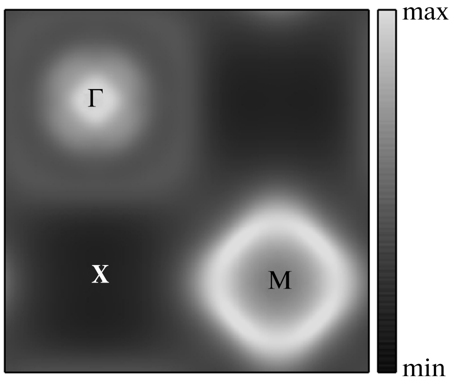

Fig. 4. Spectral density distribution map of LiFeAs in the ΓMX plane of reciprocal space as calculated by LDA+DMFT

regions of the FS do not fit under translation. This confirms suggestion that there is no (π,π) nesting in LiFeAs peculiar to other pnictides.

In conclusion, by employing the LDA+DMFT approach we have shown that local dynamical Coulomb correlations are essential part of the physics defining spectral properties of LiFeAs. The calculated single-particle **k**-integrated and **k**-resolved spectral functions are in good agreement with experimental ARPES data of Borisenko et al. [11]. The band structure calculated within DMFT in the vicinity of the Fermi energy represents the renormalized LDA bands with the computed average m^*/m as a scaling factor.

The authors thank P. Werner and J. Kuneš for providing the CT-QMC code used in our calculations. This work was supported by the Russian Foundation for Basic Research (Projects # 10-02-00046, 12-02-91371-CT_a). S.L.S. is grateful to the Dynasty Foundation.

1. Y. Kamihara, H. Hiramatsu, M. Hirano et al., J. Am. Chem. Soc. **128**, 10012 (2006).
2. V. I. Anisimov, Dm. M. Korotin, M. A. Korotin et al., J. Phys.: Condens. Matter **21**, 075602 (2009).
3. K. Haule, J. H. Shim, and G. Kotliar, Phys. Rev. Lett. **100**, 226402 (2008).
4. M. Aichhorn, L. Pourovskii, V. Vildosola et al., Phys. Rev. B **80**, 085101 (2009).
5. S. L. Skornyakov, A. V. Efremov, N. A. Skorikov et al., Phys. Rev. B **80**, 092501 (2009).
6. S. L. Skornyakov, N. A. Skorikov, A. V. Lukoyanov et al., Phys. Rev. B **81**, 174522 (2010).
7. S. L. Skornyakov, A. A. Katanin, and V. I. Anisimov, Phys. Rev. Lett. **106**, 047007 (2011).
8. I. A. Nekrasov, Z. V. Pchelkina, and M. V. Sadovskii, JETP Letters **88**(2), 144 (2008); M. V. Sadovskii, Phys.-Usp. **51**, 1201 (2008).

9. J. Ferber, K. Foyevtsova, R. Valenti, and H. O. Jeschke, Phys. Rev. B **85**, 094505 (2012).
10. J. H. Tapp, Z. Tang, B. Lv et al., Phys. Rev. B **78**, 060505 (2008).
11. S. V. Borisenko, V. B. Zabolotnyy, D. V. Evtushinsky et al., Phys. Rev. Lett. **105**, 067002 (2010).
12. M. J. Pitcher, D. R. Parker, P. Adamson et al., Chem. Commun. **45**, 5918 (2008).
13. S. Maiti, M. M. Korshunov, T. A. Maier et al., Phys. Rev. B **84**, 224505 (2011).
14. S. Maiti, M. M. Korshunov, and A. V. Chubukov, Phys. Rev. B **85**, 014511 (2012).
15. V. I. Anisimov, A. I. Poteryaev, M. A. Korotin et al., J. Phys.: Condens. Matter **9**, 7359 (1997); K. Held, I. A. Nekrasov, G. Keller et al., Phys. Status Solidi B **243**, 2599 (2006).
16. W. Metzner and D. Vollhardt, Phys. Rev. Lett. **62**, 324 (1989).
17. V. I. Anisimov, D. E. Kondakov, A. V. Kozhevnikov et al., Phys. Rev. B **71**, 125119 (2005).
18. http://elk.sourceforge.net/.
19. P. Werner, A. Comanac, L. de' Medici et al., Phys. Rev. Lett. **97**, 076405 (2006).
20. A. I. Liechtenstein, V. I. Anisimov, and J. Zaanen, Phys. Rev. B **52**, R5467 (1995).
21. P. H. Dederichs, S. Blügel, R. Zeller, and H. Akai, Phys. Rev. Lett. **53**, 2512 (1984); O. Gunnarsson, O. K. Andersen, O. Jepsen, and J. Zaanen, Phys. Rev. B **39**, 1708 (1989); V. I. Anisimov and O. Gunnarsson, Phys. Rev. B **43**, 7570 (1991).
22. J. H. Vidberg and J. E. Serene, J. Low Temp. Phys. **29**, 179 (1997).